

A Microstructure-Based Time-Dependent Crack Growth Model for Life and Reliability Prediction of Turbopropulsion Systems

KWAI S. CHAN, MICHAEL P. ENRIGHT, JONATHAN MOODY,
and SIMEON H.K. FITCH

The objective of this investigation was to develop an innovative methodology for life and reliability prediction of hot-section components in advanced turbopropulsion systems. A set of generic microstructure-based time-dependent crack growth (TDCG) models was developed and used to assess the sources of material variability due to microstructure and material parameters such as grain size, activation energy, and crack growth threshold for TDCG. A comparison of model predictions and experimental data obtained in air and in vacuum suggests that oxidation is responsible for higher crack growth rates at high temperatures, low frequencies, and long dwell times, but oxidation can also induce higher crack growth thresholds (ΔK_{th} or K_{th}) under certain conditions. Using the enhanced risk analysis tool and material constants calibrated to IN 718 data, the effect of TDCG on the risk of fracture in turboengine components was demonstrated for a generic rotor design and a realistic mission profile using the DARWIN[®] probabilistic life-prediction code. The results of this investigation confirmed that TDCG and cycle-dependent crack growth in IN 718 can be treated by a simple summation of the crack increments over a mission. For the temperatures considered, TDCG in IN 718 can be considered as a K-controlled or a diffusion-controlled oxidation-induced degradation process. This methodology provides a pathway for evaluating microstructural effects on multiple damage modes in hot-section components.

DOI: 10.1007/s11661-013-1971-9

© The Minerals, Metals & Materials Society and ASM International 2013

I. INTRODUCTION

HOT-SECTION components in advanced turbopropulsion systems are expected to operate at higher heat dwell conditions for longer time durations than those in current service conditions. Under high heat dwell environments, advanced Ni-based superalloys intended for engine disk applications may be susceptible to the occurrence of concurrent time-dependent damage modes such as creep, stress corrosion, and stress rupture in addition to cycle-dependent fatigue crack initiation and growth, which often manifest synergetic interaction effects on crack growth rates. Current life-prediction methodologies, however, generally do not treat synergetic interactions of multiple damage modes on component life reliability. Thus, there is a need to develop a probabilistic time-dependent fracture mechanics analysis capability for treating multiple damage modes in advanced Ni-based alloys for operations with long duration at high temperatures where time-dependent degradation mechanisms such as creep, oxidation, corrosion, and stress rupture may compete with time-

independent fatigue crack growth as the component life-limiting mechanism.

To address this technology need, Elder Research Inc. (Elder), Charlottesville, VA, and Southwest Research Institute[®] (SwRI[®]), San Antonio, TX, conducted a methodology development program,^[1] which focused on modeling the effects of competing time-dependent damage modes including creep, stress corrosion, and stress rupture on long-term performance and reliability of engine disks made from Ni-based superalloys that could exhibit location-specific microstructures, microstructural variability or evolution of microstructures after thermal exposures at elevated temperatures for extended time periods. One particular damage mode of interest was stress corrosion in the form of environmentally-enhanced crack growth, schematically shown in Figure 1, caused by ingress of oxygen and material degradation by oxide formation along grain boundaries. A generic fracture algorithm for treating time-dependent crack growth (TDCG) was integrated with a commercial probabilistic life-prediction code, called DARWIN[®],^[2] to complement a suite of existing capabilities including finite element analysis tools, fracture mechanics analysis tools, and reliability analysis tools. This enhancement was utilized to demonstrate the potential use of such an analysis tool for estimating part life and reliability of a turbo engine subjected to aggressive mission profiles that contain long durations at high peak and dwell temperatures, which could lead to time-dependent damage modes such as creep, corrosion, and stress rupture.

KWAI S. CHAN, Institute Scientist, MICHAEL P. ENRIGHT, Staff Engineer, and JONATHAN MOODY, Research Engineer, are with the Southwest Research Institute, San Antonio, TX 78238. Contact e-mail: kchan@swri.edu SIMEON H.K. FITCH, Director, is with the Elder Research Inc., Charlottesville, VA 22903.

Manuscript submitted April 1, 2013.

The development of the TDCG methodology proceeded in three areas, which included: (1) development of a microstructure-based TDCG model, (2) assessment of variability of pertinent material parameters in the TDCG model, and (3) DARWIN simulations to assess of the effects of pertinent random variables on fatigue life and fracture risk of a turbo-propulsion component subjected to simulated dwell fatigue conditions. In this paper, we describe the development of the microstructure-based TDCG model and examine the role that several material or microstructural parameters play in the TDCG process. The TDCG model is then coupled with a cycle-dependent crack growth model to treat dwell fatigue in Ni-based superalloys using IN 718 as a model material. Potential application of the approach for assessing life and reliability of turbo-propulsion systems under high heat dwell conditions are illustrated through DARWIN simulations.

II. TIME-DEPENDENT CRACK GROWTH MODELS

A. *K*-Controlled Crack Growth

A microstructure-based TDCG model is developed by considering the presence of an environmentally affected zone that forms within a monotonic plastic zone ahead of a crack tip subject to an applied stress intensity factor, K , as depicted in Figure 2. A crack-tip element of height, d , and width, s , is depicted in Figure 2 as the fracture process zone where environmentally induced crack growth occurs. It is envisioned that oxidation of the crack-tip element leads to a crack growth rate, da/dt , that is given by

$$\frac{da}{dt} \propto \frac{\Delta a}{\Delta t} \propto \frac{s}{t_f} \quad (1)$$

where t_f is the failure time of crack-tip element, and the crack extension, Δa , corresponds to the width of the crack-tip element, s . Fracture of the crack-tip element due to oxidation-induced fracture under a sustained applied load or K is considered to be governed by a plastic strain failure locus as shown schematically in Figure 3. For plastic strains greater than a threshold

(ϵ_{ox}), the crack-tip plastic strain and the time-to-fracture is postulated to be governed by

$$\epsilon^p$$

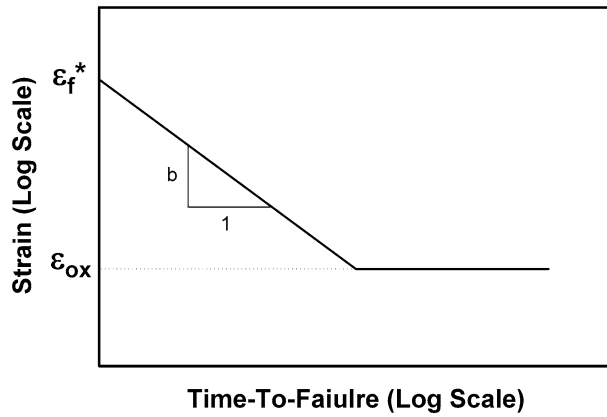


Fig. 3—Failure criteria of the crack-tip element as a function of time-to-rupture in a log-log plot.

$$\frac{da}{dt} \frac{1}{4} \frac{s_o}{t_o} \left(\frac{\pi E}{2\sigma_y \epsilon_f} \right)^{m/2} \left(\frac{1}{E \pi d_o} \right)^m \left(\frac{D_o}{D} \right)^{m\gamma/2} \exp \left(\frac{Q}{RT} \right) K^m \quad \text{14}$$

where D is the grain size, $m = 1/b$, is a constant equal to 1/3 (for IN 718), and the parameter with subscript o represents the reference value of the grain size and the crack-tip element size.

To verify the model, Eq. [4] was integrated with time to derive a relation between K , grain size, and the time-to-rupture. The analysis showed that the governing equation is given by

$$KD^{1/2} t_f^{1/m} \frac{1}{4} c \quad \text{15}$$

where c is a constant. Equation [5] predicts that the initial K value for causing stress rupture or creep rupture increase with increasing grain size. This type of experimental data was previously reported for a Ni-based superalloy, IN 792, by Larson and Floreen.^[4] Their results for powder-metallurgy (PM), cast and wrought (C&W) IN 792 materials with smooth or serrated grain boundaries are presented in Figure 4. The measured slope for the PM IN 792 is about 0.48, which appears to support the theoretical slope of 0.5 based on Eq. [5].

Time-dependent crack growth under K-controlled conditions is often expressed as

$$\frac{da}{dt} \frac{1}{4} B_o \exp \left(\frac{Q}{RT} \right) K^m \quad \text{with } m > 0 \text{ and } K > K_{th} \quad \text{16}$$

where K_{th} is the crack growth threshold and B_o is an empirical constant. Comparing Eqs. [4] and [6] indicates that the empirical constant B_o incorporates all of the material parameters according to the relation given by

$$B_o \frac{1}{4} \frac{s_o}{t_o} \left(\frac{\pi E}{2\sigma_y \epsilon_f} \right)^{m/2} \left(\frac{1}{E \pi d_o} \right)^m \left(\frac{D_o}{D} \right)^{m\gamma/2} \quad \text{17}$$

which depends on the underlying microstructure but not on the temperature, stress, or the stress intensity factor, K .

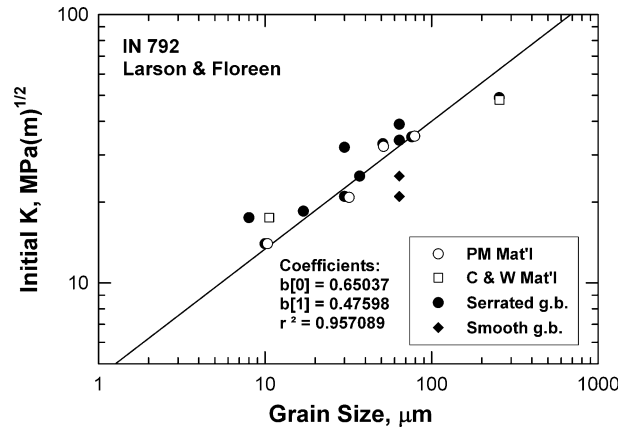


Fig. 4—The initial K value required to cause failure of IN 792 in 100 h under a sustained applied load as a function of grain size. The experimental data are from Larson and Floreen.^[4]

B. Diffusion-Controlled Crack Growth Model

Time-dependent crack growth under diffusion-controlled conditions can be obtained from Eq. [4] by setting $m = 0$ so that da/dt is independent of the applied K level, which is a characteristic of the diffusion-controlled crack growth. Applying this constraint to Eq. [4] leads one to

$$\frac{da}{dt} \frac{1}{4} \frac{s_o}{t_o} \exp \left(\frac{Q}{RT} \right) \quad \text{18}$$

which becomes applicable when the crack-tip plastic strain is insufficient to cause fracture of the oxide film formed at the crack tip on the crack surfaces. Under this circumstance, crack growth is controlled by diffusion of oxygen through the crack-tip oxide film. Applying $m = 0$ to Eq. [7] leads one to $B_o = s_o/t_o$ for diffusion-controlled crack growth. A microstructure-based model for C_t -controlled crack growth, where C_t is the transient creep crack growth parameter, is currently in development.

The transition from K-controlled TDCG to diffusion-controlled TDCG in IN 718 was identified and summarized in Figure 5. The da/dt data of IN 718 from three different sources are compared in Figure 5. A power-law with an m -exponent of 3 is observed in the Pratt & Whitney (PW) material for the Probabilistic Design for Rotor Integrity Program.^[5] In contrast, an m -exponent of 1.6 to 2 is observed in the materials used in the studies by Pedron and Pineau,^[6] and Gao *et al.*^[7] At high K levels, the m -exponent in IN 718 decreases with increasing K and the crack growth rate appears to become constant when $K > 48 \text{ MPa(m)}^{1/2}$. A constant da/dt appears to be achieved in IN 100 + Nb,^[8] which was tested in pure oxygen. A comparison of the different m values observed in these alloys is presented as a function of K in Figure 6. High m values are observed in the near-threshold region at low K levels. A constant slope or m value in the range of 2 to 3 is observed above the threshold. At high K levels, the m value decreases to less than 1 and approaches to zero in the IN 718 material

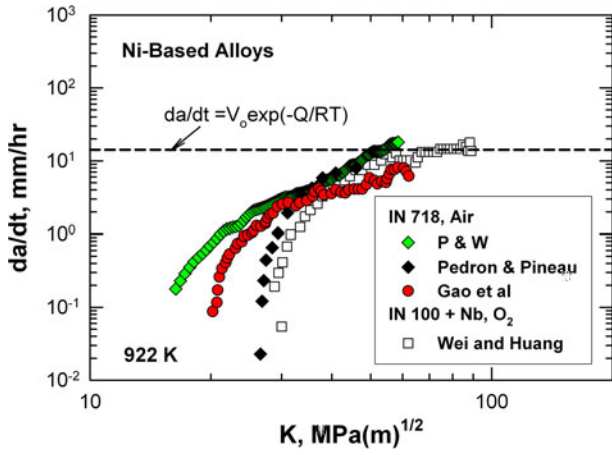


Fig. 5—Time-dependent crack growth rate, da/dt , as a function of stress intensity factor for IN 718 and IN 100+Nb at 922 K (1200°F). Experimental data are from PW,^[5] Pedron and Pineau,^[6] Gao *et al.*,^[7] and Wei and Huang.^[8]

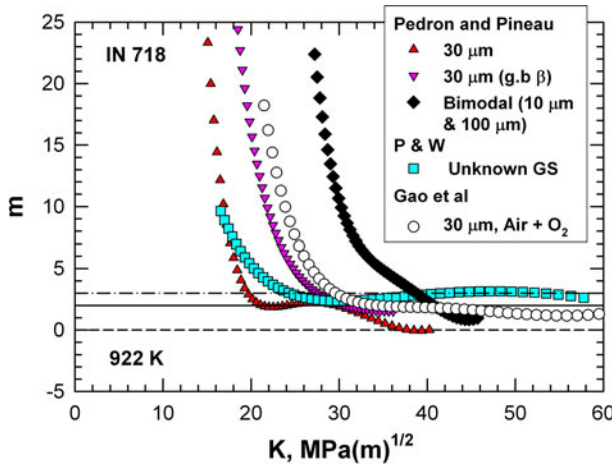


Fig. 6—The crack growth exponent, m , as a function of K observed in IN 718 with different microstructure from several sources.^[5-7]

studied by Pedron and Pineau.^[6] The results suggested that diffusion-controlled TDCG, which can be identified by $m = 0$, occurs in IN 718 with certain microstructures at K levels greater than about $49 \text{ MPa(m)}^{1/2}$. The transition from K -controlled to diffusion-controlled crack growth occurs with an abrupt change of the m value from about 3 to 0. A steady-state diffusion-controlled crack growth with $m = 0$ has not been reported for IN 718, but appears to occur in IN 100 with Nb in oxygen.^[7,8] In order to develop a generalized model, diffusion-controlled crack growth was assumed to occur in IN 718 at high K levels ($>49 \text{ MPa(m)}^{1/2}$).

III. VARIABILITY OF MATERIAL PARAMETERS

An inspection of Eqs. [4], [6], and [8] indicated that material parameters that affect the TDCG rate, da/dt , include the activation energy (Q), the crack-growth

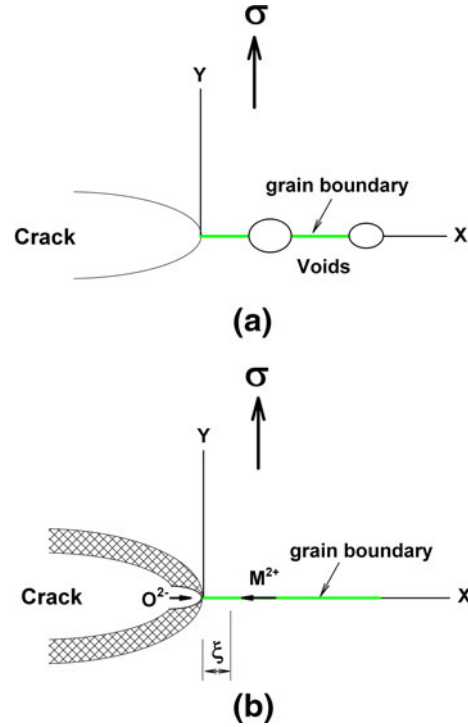


Fig. 7—Schematics of creep crack growth and oxidation-induced crack growth: (a) creep crack growth by grain-boundary cavitation, and (b) oxidation along grain boundary. Both processes proceed by grain boundary diffusion.

exponent (m), the crack growth threshold, K_{th} , grain size (D), and the yield stress, σ_y . In this paper, we will focus on the effects of microstructure on Q , m , and K_{th} .

A. Activation Energy for Oxidation

The activation energy for TDCG in Ni-based superalloys is investigated by considering the pertinent controlling crack-tip fracture processes. In vacuum, TDCG in Ni-based alloys has been shown to proceed by the growth of creep-induced cavities along grain boundaries and the activation energy corresponds to that for grain boundaries diffusion,^[9-11] as shown schematically in Figure 7(a). In air environments, TDCG is at least partly, if not totally, controlled by the kinetics of oxide formation at the crack tip,^[6,7,9-17] which is illustrated in Figure 7(b). The oxide growth at the crack surface and the crack tip can be described either by a linear growth law if the oxides are non-protective or by a parabolic growth law if the oxide film is protective.^[18] A generalized oxide growth law controlled by grain boundary diffusion is given by

$$\xi \propto k_{po} \exp\left(-\frac{Q_{gb}}{RT}\right) t^{\alpha_o} \quad (9)$$

where ξ is the oxide thickness, k_{po} is the oxide growth constant, Q_{gb} is the activation energy for grain boundary diffusion, R is the universal gas constant, T is absolute temperature, and α_o is the oxide growth exponent with $\alpha_o = 1$ for linear growth and $\alpha_o = 1/2$ for

parabolic growth. Differentiation of Eq. [9] gives the oxide thickening rate as

$$\frac{d\xi}{dt} \approx \frac{\alpha_o k_{po}^{1/\alpha_o}}{\xi^{1/\alpha_o - 1}} \exp\left(-\frac{Q_{gb}}{\alpha_o RT}\right) \quad \text{Eq. 10}$$

which leads to

$$\frac{da}{dt} \approx \frac{\alpha_o k_{po}^{1/\alpha_o}}{\xi_c^{1/\alpha_o - 1}} \exp\left(-\frac{Q_{gb}}{\alpha_o RT}\right) \quad \text{Eq. 11}$$

when the oxide film fractures and the crack extends after the thickness exceeds a critical thickness, ξ_c . Taking natural logarithm of Eq. [11] gives

$$\ln \frac{da}{dt} \approx \ln \frac{\alpha_o k_{po}^{1/\alpha_o}}{\xi_c^{1/\alpha_o - 1}} - \frac{Q_{gb}}{\alpha_o RT} \quad \text{Eq. 12}$$

which indicates that in a plot of $\ln da/dt$ vs $1/T$, the apparent activation energy, Q_{app} , is related to the linear slope, β , according to the expression given by

$$\beta \approx \frac{Q_{gb}}{\alpha_o R} \approx \frac{Q_{app}}{R} \quad \text{Eq. 13}$$

leading to

$$Q_{app} \approx \frac{Q_{gb}}{\alpha_o} \quad \text{Eq. 14}$$

for crack growth governed by a generalized oxide growth law. For cracking of an oxide film exhibiting a linear growth law, $\alpha_o = 1$ and $Q_{app} = Q_{gb}$. For cracking of a protective oxide film (such as Al_2O_3 and Cr_2O_3) exhibiting a parabolic oxide growth law ($\alpha_o = 1/2$), $Q_{app} = 2Q_{gb}$. Three key results of this analysis are: (1) the activation energy associated with TDCG involving linear oxide growth is Q_{gb} , which is identical to that of creep crack growth in vacuum, (2) the activation energy associated with TDCG involving parabolic oxide growth is $2Q_{gb}$, which typically corresponds to the volumetric diffusion coefficient, and (3) a range of Q_{app} values from Q_{gb} to $2Q_{gb}$ may be expected for mixed oxide growth or if the protective oxide film is repeatedly fractured so that oxide growth oscillates between linear and parabolic growth. The various possible Q_{app} values and the corresponding oxidation kinetics are illustrated schematically in Figure 8.

The activation energy, Q , for TDCG of IN 718 was investigated by plotting da/dt data^[4,5,12-16] as a function of the reciprocal temperature in a semi-log plot as shown in Figure 9. The slope of the linear line is Q/R , where Q is the activation energy and R is the universal gas constant. Available da/dt data for IN 718 tested in vacuum,^[11] air,^[4,5,12-15] moist argon,^[16] and oxygen^[16] from the literature are summarized and presented in Figure 9. A summary of the Q values deduced from the regression fit of the literature data is presented in Table I, which shows there is variability in the Q value among all of the different sets of da/dt data for IN 718 in vacuum, air, moist argon, and oxygen. The results for IN 100 + Nb (5 wt pct)^[8] were also included in Table I because this alloy behaved like IN 718 with the addition

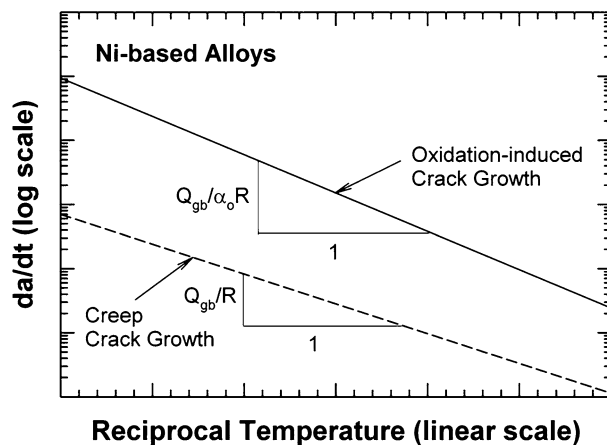


Fig. 8—Schematic shows the effects of linear ($\alpha_o = 1$) and parabolic ($\alpha_o = 1/2$) oxidation kinetics on the activation energy for oxidation-induced crack growth in air compared to creep crack growth by grain boundary diffusion in vacuum.

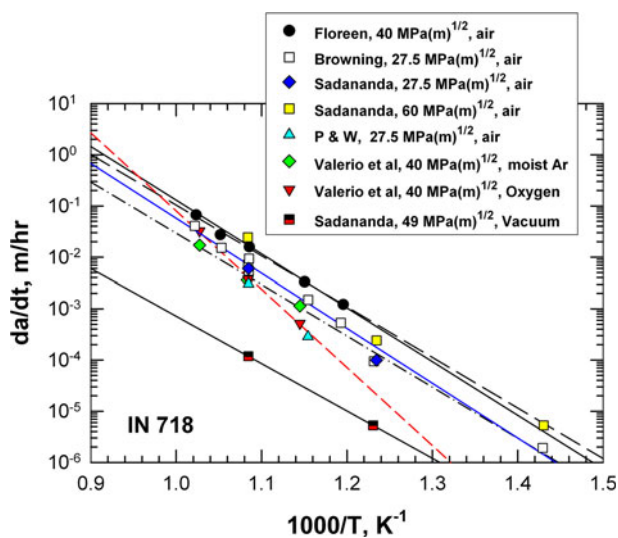


Fig. 9—A semi-log plot of da/dt vs reciprocal temperature shows variations in the slope (Q/R) for IN 718 in vacuum,^[11] air,^[4,5,12-15] moist argon,^[16] and oxygen^[16] environments. The da/dt data are from Refs. [4], [5], and [11-16].

of 5 wt pct Nb. The lowest Q value, $Q_{vac} = 178$ kJ/mol, was associated with creep crack growth in IN 718 in vacuum,^[11] which was controlled by grain boundary diffusion and cavitation. All of the Q values for oxidation-induced crack growth in IN 718 tested in air are either larger or substantially larger than the Q value in vacuum.

Analysis of the oxidation kinetics revealed that linear oxidation kinetics would lead to a Q value that is similar to that in vacuum when oxidation is controlled by grain boundary diffusion. In contrast, an apparent Q value of $2Q_{vac}$ is expected when oxidation is parabolic and controlled by diffusion through a protective oxide film. Furthermore, a range of Q values from Q_{vac} to $2Q_{vac}$ can be expected in the case of mixed oxide formation ahead of the crack tip. Thus, the range of Q values observed in

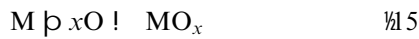
Table I. Summary of the Activation Energy, Q , for TDCG in IN 718 and IN 100 + Nb In Vacuum, Air, Moist Argon, and Oxygen Environments

| Alloy | Environment | K (MPa(m) ^{1/2}) | Q (kJ/g mol) | Source |
|-------------|-------------|------------------------------|----------------|---------------------------------------|
| 718 | vacuum | 49 | 178.06 | S&S ^[11] |
| IN 718 | air | 27.5 | 348.8 | PW ^[5] |
| | air | 40 | 189.11 | Floreen ^[12] |
| | air | 27.5 | 204.79 | Browning ^[13] |
| | air | 60 | 200.54 | S&S ^[14] |
| | air | 27.5 | 281.30 | S&S ^[15] |
| | moist argon | 40 | 191.12 | Valerio <i>et al.</i> ^[16] |
| IN 100 + Nb | oxygen | 40 | 291.59 | Valerio <i>et al.</i> ^[16] |
| | oxygen | 60 | 289.42 | Wei & Huang ^[8] |

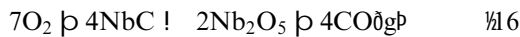
the experimental data of IN 718 in Figure 9 and in Table I, may be attributed to oxidation kinetics that vary from linear growth to parabolic growth or mixed oxide growth.

B. Time-Dependent Crack Growth Threshold

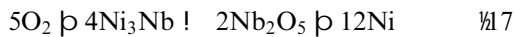
The threshold, K_{th} , for K -controlled TDCG is defined as the stress intensity factor above which the onset of TDCG occurs at the tip of a Mode I crack subjected to a sustained static load. At K levels below K_{th} , the sustained loaded crack does not extend in length but the degradation process such as oxidation, corrosion or creep may remain active. For illustration purposes, Figure 10 depicts the formation of an oxide layer as the result of inward diffusion of oxygen along a grain boundary located ahead of the crack tip. It is envisioned that oxygen would react with the metallic matrix phase, metal carbide or an intermetallic to form oxide particles at the grain boundary. For example, a certain element, M , in the Ni solid-solution phase to form MO according to the reaction given by References 9 and 10



where M can be Ni, Cr, Co, Ti, Al or Nb and x can be 1, 3/2, 2, or 5/2, depending on M . In addition, NbC and Ni_3Nb can react with oxygen to form Nb_2O_5 according to the reaction given by References 7, 8, 16



or



which indicates that the oxidation products in the crack-tip process zone may include oxide formation that involves a volume change (transformation strain) and, among others, the formation of a gaseous phase (CO) that may exert pressure on the crack surface.

The formation of a volume-expanding oxide in the crack-tip process zone can induce compressive transformation stresses and results in crack-tip shielding similar to that observed in phase-transformation toughening.^[19] In contrast, the formation of a volume shrinkage phase can induce tensile transformation stress and crack-tip anti-shielding that promote fracture of the transformed oxide phase. At the crack growth threshold, the applied

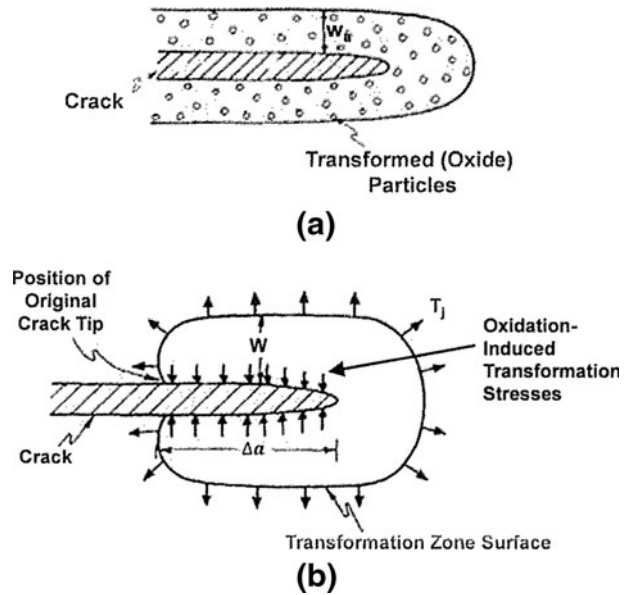


Fig. 10—Schematics of transformation toughening associated with the formation of a volume expanding oxide in the crack-tip process zone: (a) oxidation-induced transformation zone of oxide particles, and (b) oxidation-induced compressive transformation stresses acting to close the main crack tip. Modified from McMeeking and Evans.^[19]

stress intensity factor must overcome the fracture toughness of the oxide and the crack-tip shielding due to the oxidation-induced compressive stresses. Applying the theory of transformation toughening to oxide formation at the crack tip leads one to Reference 19

$$K_{th} \text{ } \rho \text{ } K_{ox} \text{ } \rho \text{ } \frac{0.22}{\partial l} \varepsilon^T E V_f \frac{\rho}{w} \quad \rho \text{ } 8$$

where ε^T is the transformation strain, E is the elastic modulus of the transformed phase (*i.e.*, oxide), ν is the Poisson's ratio, V_f is the volume fraction of the transformed phase (*e.g.*, oxides), and w is the width of the transformation (oxidation) zone. The second term on the right-hand-side of Eq. [18] is the transformation toughening term associated with the formation of an oxide product with a transformation strain. Besides Nb_2O_5 ,^[7,8,16] other oxides that may form in Ni-based superalloys with a transformation strain include MO (NiO , CrO , CoO), Al_2O_3 , Cr_2O_3 , TiO_2 , and

Table II. Summary of the Compound, Crystal Structure, Lattice Parameter, Unit Cell Volume, Elastic Modulus (E), and Fracture Toughness (K_{IC}) of Individual Constituent Phases Pertinent for Consideration of Oxidation-Induced Transformation Toughening in Ni-Based Alloys

| Compound | Crystal Structure | Lattice Parameters (Å) | Unit Cell Volume (Å ³) | E (GPa) | K_{IC} (MPa(m) ^{1/2}) |
|----------------------------------|-------------------|--|------------------------------------|-------------------------------|-----------------------------------|
| Ni _{ss} | fcc | $a_o = 3.529$ ^[22] | 41.61 | 200 ^[44] | 96 to 131 ^[45] |
| NbC | fcc | $a_o = 4.470$ ^[25,26] | 93.91 | 340 to 400 ^[28] | 3.0 to 4.0 ^[28] |
| Ni ₃ Nb | bct | $a_o = 3.655$; $c_o = 7.495$ ^[22,23] | 100.13 | 200 | 6.0 to 8.0 ^[29] |
| M ₆ C | cubic | $a_o = 10.62$ ^[25] | 1197.8 | — | 7.1 ^[30] |
| M ₂₃ C ₆ | cubic | $a_o = 10.63$ ^[25,27] | 1201.2 | 325 to 334 ^[31] | 7.1 ^[30] |
| Ni ₃ Al | cubic | $a_o = 3.57$ to 3.60 ^[22–24] | 45.5 | 178 ^[32] | 30 ^[32] |
| Cr ₂ O ₃ | hcp | $a_o = 4.961$; $c_o = 13.6$ ^[36] | 289.87 | 143.6 ^[33] | 3.6 ^[33] |
| Al ₂ O ₃ | hcp | $a_o = 4.785$; $c_o = 12.991$ ^[37] | 257.59 | 362 ^[28,33] | 3.5 ^[28,33] |
| TiO ₂ | tetragonal | $a_o = 3.784$; $c_o = 9.514$ ^[38] | 136.27 | 270.7 ^[33] | 2.49 ^[33] |
| Nb ₂ O ₅ | hcp | $a_o = 3.607$; $c_o = 3.925$ ^[39] | 44.22 | 125 ^[34] | 1.5 |
| CoO | cubic | $a_o = 4.254$ ^[40,41] | 75.44 | 189 ^[35] | 1.12 ^[35] |
| NiO | cubic | $a_o = 4.173$ ^[40,41] | 72.67 | 230 to 260 ^[35,36] | 1.5 ^[35,46] |
| CrO | cubic | $a_o = 4.1$ ^[42] | 68.92 | — | 1.5 |
| NiCr ₂ O ₄ | cubic | $a_o = 8.32$ ^[43] | 573.9 | 106.6 ^[35] | 0.57 ^[35] |

NiCr₂O₄.^[9,10,20,21] These oxides may form when oxygen reacts with metallic carbides, intermetallics, or the Ni solid-solution matrix that contains these alloying elements.

To assess the applicability of Eq. [18] to Ni-based superalloys, the crystal structure, lattice parameters, Young's modulus (E), and K_{ox} , for selected oxides, carbides, and intermetallics are compiled from the literature and the results are presented in Table II. The fracture toughness of oxides in bulk form are typically in the range of 0.5 to 4 MPa(m)^{1/2},^[33,35,36] while the K_{th} values for IN 718, which are about 14 MPa(m)^{1/2}^[5] or greater,^[6–8] as shown in Table III, are much larger than the fracture toughness of the bulk oxides. This finding suggests that transformation toughening may indeed occur during oxide formation and growth in the crack-tip process zone during sustained-loaded crack growth. The oxidation reactions given by Eqs. [12] to [14] were utilized to compute the transformation strain on the basis of the unit-cell volumes of the reactant and the product and the results are summarized in Table IV. The values of $(K_{th} - K_{ox})/V_f$, which measures the change in the FCG threshold per unit volume fraction of oxide, were computed on the basis of a transformation-zone width of 1 μ m are shown in Column 7 of Table IV. Estimates of K_{th} based on $V_f = 0.25$ and $w = 1 \mu$ m are computed for various oxides and the results are presented in the last column of Table IV.

The results shown in Table IV indicate that the transformation strains for the various oxides formed as the result of the oxidation of metallic elements from the solid-solution phase or Ni₃Al all being positive, meaning the oxide product exhibits a larger volume than the metallic reactant oxidized by oxygen. The result is the inducement of compressive residual stress in the oxidation process zone, crack-tip shielding, and an enhanced K_{th} that is considerably larger than K_{ox} , as shown in Table IV. When the reactants are carbides or Ni₃Nb, the transformation strains are negative, meaning the oxide product exhibits a smaller volume than the reactants (carbides or Ni₃Nb). The consequence is the creation of tensile residual stresses in the oxidation

Table III. Summary of K_{th} for TDCG and ΔK_{th} (at $R = 0.1$) for Cycle-Dependent Crack Growth in IN 718

| T [K (°C)] | K_{th} (MPa(m) ^{1/2}) | ΔK_{th} (MPa(m) ^{1/2}) |
|--------------|-----------------------------------|--|
| 297 (24) | — | 8.2 ^[47] |
| 811 (538) | 14.8 ^[5] | — |
| 866 (593) | 14.8 ^[5] | 8.2 ^[47] |
| 923 (650) | 14.3 ^[5] | 7.7 ^[47] |
| 923 (650) | 18 to 26 ^[6] | 6.8 to 7.9 ^[48] |

process zone, crack-tip anti-shielding, and a reduced K_{th} that is smaller than the fracture toughness of the oxide, K_{ox} . For many carbides, the tensile residual stresses are so large that the computed K_{th} actually has a negative value, meaning the transformed oxide would be fractured instantly at an apparent value of zero for K_{th} . These findings indicate that oxidation of the Ni solid-solution matrix phase is less damaging than oxidation of the grain boundary carbides and Ni₃Nb since matrix oxidation can lead to a higher apparent K_{th} by virtue of transformation toughening.

A summary of the K_{th} values reported in the literature for IN 718 is presented in Table III. For IN 718, the K_{th} value ranges from 14 to 26 MPa(m)^{1/2}.^[5–8] This range of K_{th} values is consistent with the observation that NiO and Cr₂O₃ are the common oxides associated with TDCG in IN 718.^[9,10,20] Segregation of Nb to the grain boundaries and the formation of Nb₂O₅ have also been reported,^[7,8,16,17] as well as the release of CO during TDCG in IN 718.^[7] In general, a mixture of oxides may form from reactants such as Ni solid-solution phase, grain boundary carbides, and intermetallics.^[7–10,16,17,20] The variation in the underlying oxidation mechanism leads to a wide range of K_{th} values with a substantial scatter for IN 718 and other Ni-based superalloys.

Besides oxide-induced transformation toughening, the presence of an oxide film or layer on the crack surface can cause oxide-induced crack closure (OICC) of a fatigue crack subjected to cyclic loading. The reduction in the stress intensity factor, ΔK_{OICC} , due to OICC was

Table IV. Summary of the Reactant, Oxide Product, Unit Cell Volumes, Elastic Modulus of Oxide (E_{ox}), Transformation Strain (e^T), and Computed K_{th} Values Based on $w = 1 \mu\text{m}$ and $V_f = 0.25$

| Reactant | Oxide Product | Unit Cell Volume, \AA^3 Reactant | Unit Cell Volume, \AA^3 Product | E_{ox} (GPa) | $e^T = \Delta V/V$ | $(K_{th} K_{ox})/V_f$ (MPa(m) $^{1/2}$) | K_{th} (MPa(m) $^{1/2}$) |
|-------------------------------------|----------------------------------|---|--|----------------|--------------------|--|-----------------------------|
| Cr in Ni _{SS} | Cr ₂ O ₃ | 41.61 | 289.87 | 143.6 | 5.65 | 266.4 | 70.2 |
| Al in Ni _{SS} | Al ₂ O ₃ | 41.61 | 257.59 | 361.9 | 4.91 | 583.5 | 149.4 |
| Ti in Ni _{SS} | TiO ₂ | 41.61 | 136.27 | 270.7 | 2.12 | 188.4 | 49.6 |
| Co in Ni _{SS} | CoO | 41.61 | 75.44 | 143.6 | 0.81 | 38.2 | 10.7 |
| Ni in Ni _{SS} | NiO | 41.61 | 72.67 | 260 | 0.75 | 64.0 | 17.5 |
| Cr in Ni _{SS} | CrO | 41.61 | 68.92 | 143.6 | 0.66 | 31.1 | 9.3 |
| Ni, Cr in Ni _{SS} | NiCr ₂ O ₄ | 41.61 | 573.9 | 106.6 | 4.38 | 153.3 | 38.9 |
| Al in Ni ₃ Al | Al ₂ O ₃ | 45.5 | 257.59 | 361.9 | 0.46 | 54.7 | 17.2 |
| M in M ₂₃ C ₆ | Nb ₂ O ₅ | 1201.2 | 44.22 | 125 | 0.96 | 39.4 | 8.4 |
| | Cr ₂ O ₃ | 1201.2 | 289.87 | 143.6 | 0.76 | 35.8 | 5.4 |
| Nb in Ni _{SS} | Nb ₂ O ₅ | 41.61 | 44.22 | 125 | 0.014 | 0.6 | 1.6 |
| Nb in NbC | Nb ₂ O ₅ | 93.81 | 44.22 | 125 | 0.46 | 18.9 | 3.2 |
| Nb in Ni ₃ Nb | Nb ₂ O ₅ | 98.84 | 44.22 | 125 | 0.552 | 22.7 | 4.2 |

been derived by others and is given by References 49 and 50

$$\Delta K_{OICC} \approx \frac{E h_{ox}}{4\delta l} \frac{1}{v^2 \rho} \frac{1}{\pi r_{ox}} \quad (19)$$

where h_{ox} is the oxide thickness formed on the crack surfaces in the crack wake and r_{ox} is the distance behind the crack tip over which OICC occurs. It is noted that the oxide thickness on the crack surfaces can be different from the oxide thickness, ξ in Eq. [9], formed along the grain boundaries ahead of the crack tip. Previous work has indicated that the activation energy for OICC for fatigue crack growth of large cracks in IN 718 is about 55 kJ/mol,^[51] which is significantly lower than the activation energy for grain boundary diffusion and oxide formation along grain boundaries as shown in Eq. [9]. Available experiment data in the literature indicate that the cyclic crack growth threshold, ΔK_{th} , is lower than the TDCG threshold, K_{th} , for IN 718 (Table III) and other Ni-based superalloys.^[52]

IV. COMBINED CYCLE-DEPENDENT AND TIME-DEPENDENT CRACK GROWTH

Cycle-dependent fatigue crack growth and TDCG are generally treated as two independent processes whose crack growth increment, da , over a mission can be summed according to the expression given by References 53 and 54

$$\delta da \approx \delta a_{mission} \approx \left(\frac{da}{dN} \right)_{cyclic} dN + \left(\frac{da}{dt} \right) dt \quad (20)$$

where the first term on the right-hand-side of Eq. [21] treats cycle-dependent crack growth while the second term treats TDCG for an arbitrary loading history within a mission. For fatigue crack growth test data generated under a constant frequency with dwell, Eq. [21] can be expressed as

$$\left(\frac{da}{dN} \right)_{dwell} \approx \frac{1}{4} \left(\frac{da}{dN} \right)_{cyclic} \rho^{1/2} t_{dwell} \rho^{1/f} \left(\frac{da}{dt} \right) \quad (21)$$

where t_{dwell} is the dwell time and f is the frequency. The fatigue crack growth rate, da/dN , was represented in terms of the Paris power-law,^[55] as given by

$$\frac{da}{dN} \approx A \Delta K^n \quad \text{for } \Delta K > \Delta K_{th} \quad (22)$$

where ΔK is the stress intensity range, ΔK_{th} is the large-crack growth threshold, and A and n are material constants. Cyclic crack growth generally follows a transgranular path, while TDCG due to grain boundary oxidation typically follows an intergranular path.^[56-59] The transition from transgranular fracture to intergranular fracture depends on the temperature, load frequency, and hold time, which are modeling in terms of the linear summation rule as described in Eq. [9] and the activation energy term in Eqs. [4] and [6].

V. DARWIN LIFE-PREDICTION AND RISK ASSESSMENT

Material constants for diffusion-controlled TDCG in IN 718 were evaluated and utilized in conjunction with DARWIN to assess the risk of fracture involving multiple damage modes, including K-controlled TDCG, diffusion-controlled crack growth, and cycle-dependent crack growth. Evaluation of material constants and application of the K-controlled TDCG law, Eq. [6], have been reported earlier for IN 718. Figure 11 shows a comparison of the computed and experimental da/dN and da/dt curves for IN 718 at 923 K (650 °C). In this study, emphasis is placed on the life-prediction under diffusion-controlled crack growth. Since diffusion-controlled crack growth was never actually reported for IN 718, an assumed da/dt curve was constructed on the basis of da/dt data of several studies^[2-5] that showed the crack growth rate appeared to approach a steady-state at high K levels, suggesting that a diffusion-controlled

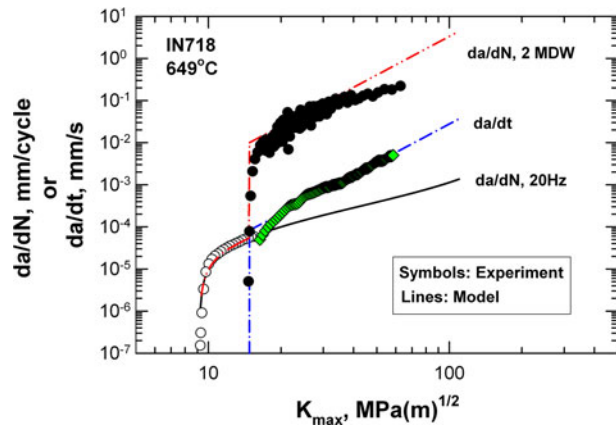


Fig. 11—Comparison of computed da/dN at 20 Hz, da/dN with two-minute dwell (2 MDW) and da/dt curves against experimental data for IN 718.

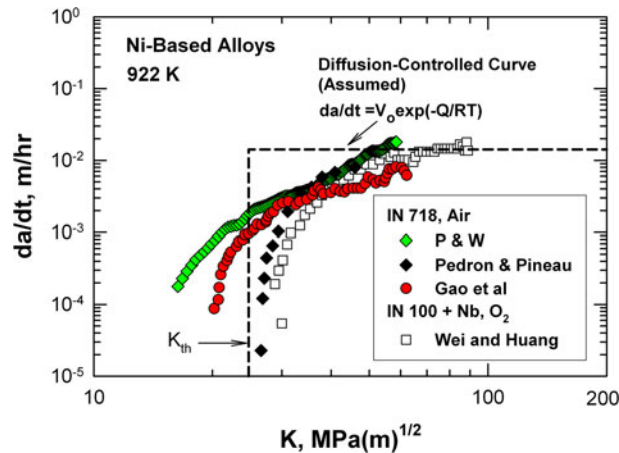


Fig. 12—Assumed da/dt curve for diffusion-controlled crack growth in IN 718 compared to experimental data from the literature.^[5-8]

crack growth region may occur at high K levels ($K > 49 \text{ MPa(m)}^{1/2}$). The K_{th} value was first taken to be $49 \text{ MPa(m)}^{1/2}$, but it produced no reduction in fatigue life. Thus, a K_{th} value of $24.7 \text{ MPa(m)}^{1/2}$, which is the mean of the available K_{th} data from the literature,^[2-5] was selected for subsequent crack growth computation. The assumed diffusion-controlled da/dt curve is compared against that for K-controlled crack growth in Figure 12 for 923 K ($650 \text{ }^\circ\text{C}$). The relevant material constants for diffusion-controlled crack growth are the crack growth threshold, K_{th} , and the activation energy, Q , which are summarized in Table V. These material constants were utilized to perform risk analysis of an IN 718 disk using DARWIN and a generic mission profile supplied by an industrial partner. It should be noted that the material parameters were chosen deliberately to exercise the diffusion-controlled crack growth model in the DARWIN code. The result of this deterministic diffusion-controlled crack growth analysis is presented in Figure 13, which shows the crack area as a function of the flight (mission). For comparison, the result for K-controlled crack growth is also presented in Figure 13.

Table V. Summary of the Mean and Standard Derivation (SD) of the K_{th} and Q Values Used in Probabilistic Crack Growth Computation Using DARWIN

| | K_{th} (MPa(m) ^{1/2}) | Q (kJ/g mol) |
|------|-----------------------------------|----------------|
| Mean | 24.75 | 241.27 |
| SD | 11.75 | 60.76 |

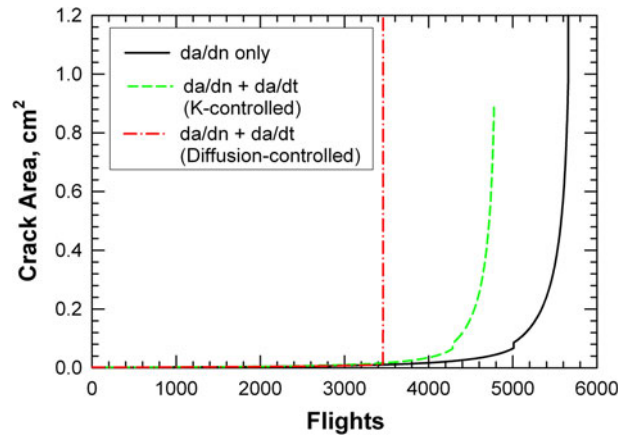


Fig. 13—Deterministic crack growth results of crack areas as a function of flight (mission) for cycle-dependent crack growth in an IN 718 disk with and without TDCG under K-controlled mode or diffusion-controlled mode.

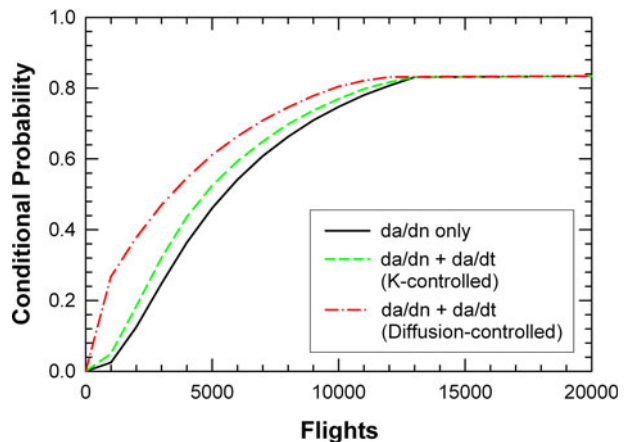


Fig. 14—Risk of disk fracture as a function of flight (mission) for cycle-dependent crack growth in an IN 718 disk with and without TDCG under K-controlled mode or diffusion-controlled mode.

The comparison indicates that the computed fatigue life is reduced by the onset of diffusion-controlled crack growth, which leads to final fracture rather abruptly once K_{th} ($K_{th} = 24.7 \text{ MPa(m)}^{1/2}$) is exceeded because crack growth due to da/dt is significantly higher than da/dN for the material parameters chosen. The corresponding risk of fracture is presented in Figure 14, which shows increased risk of fracture due to diffusion-controlled crack growth compared to cycle-dependent crack growth only. Besides verifying the da/dt algorithm in DARWIN,^[2] the crack growth computation

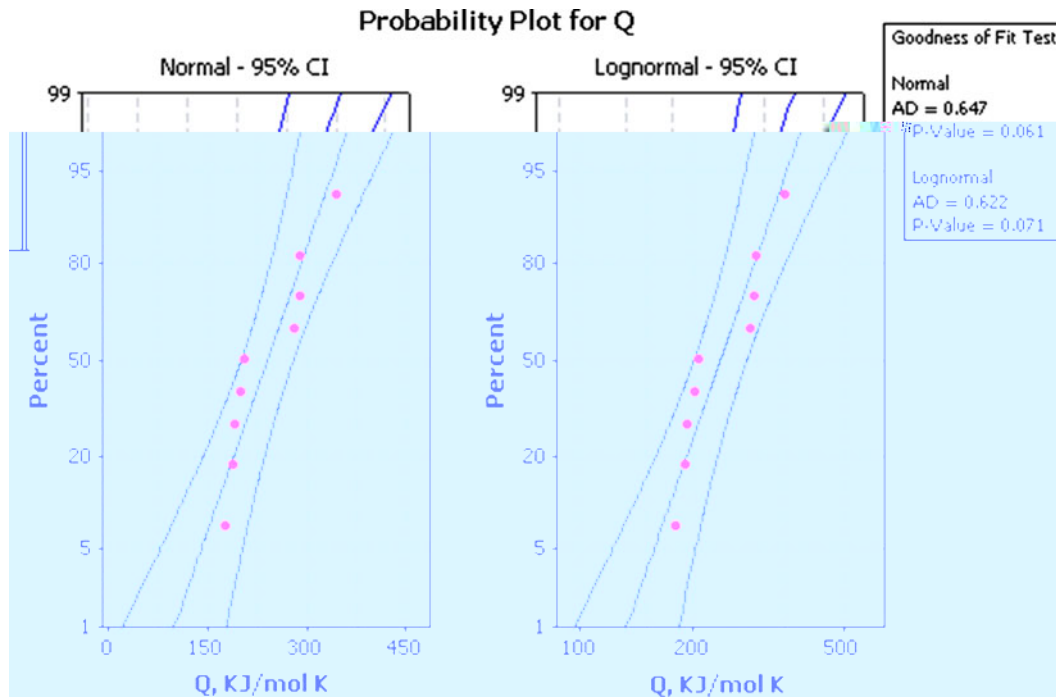


Fig. 15—Distribution of Q values for IN 718: (a) normal distribution, and (b) log-normal distribution.

demonstrated that the K_{th} value is an important material parameter that affects the crack growth life and risk of fracture for damage mode involving stress corrosion cracking, which is often manifested as a diffusion-controlled crack growth process.

The deterministic crack growth analysis was followed by a probabilistic crack growth analysis. The random variables were chosen to be K_{th} and Q because of availability of experimental data from the literature. Both Q and K_{th} are well described in terms of the log-normal distributions. Figure 15 shows the distribution of the Q values. Numerical difficulties were encountered when the Q value generated from the log-normal distribution was either too large or too small; a zero da/dt was obtained when Q was too large and an unrealistically large da/dt was obtained when Q was too small. To avoid these difficulties, the log-normal distribution of Q was truncated by a lower-bound value of 178 kJ/mol and an upper-bound value of 356 kJ/mol, which correspond to Q_{vac} and $2Q_{vac}$ for IN 718, respectively. The probability distribution functions (pdfs) for K_{th} and Q are presented in Figures 16(a) and (b), respectively. The probabilistic crack growth results based on the truncated log-normal distribution for Q are presented in Figure 17, which shows the risk of fracture as a function of flight (mission). The results computed based on the medians of K_{th} and Q is shown as a solid line labeled as no scatter. The result for Q scatter only is almost the same as that without scatter, while scatter in K_{th} leads to an increase in the risk of disk fracture. The effect of Q scatter on the risk of fracture is very limited because the lower bound has been set at 179 kJ/mol, which corresponds to the activation energy for crack growth controlled by grain boundary diffusion. Reducing the lower bound Q value implies the

activation of additional damage mechanisms. For example, the activation energy for hydrogen embrittlement in ALLVAC 718Plus has been reported to be 40 kJ/mol^[56] or other damage mechanisms with lower apparent activation energy have also reported for Ni-based alloys.^[57] The low end of the Q distribution curve, which implies the occurrence of a degradation mechanism such as hydrogen embrittlement, is inconsistent with the experimental observation of high K_{th} values for most Ni-based alloys in general and IN 718 in particular. A low Q value typically leads to an unrealistically high da/dt and premature fracture. For this reason, the low end of the Q distribution curve needs to have a cutoff that is commensurate with the experimentally observed degradation mechanisms, and certain low Q values, such as those for hydrogen embrittlement, need to be excluded if these degradation mechanisms do not occur under service conditions. For IN 718, a reasonable cutoff appears to be the activation for grain boundary diffusion, Q_{gb} ($Q_{gb} = 179$ kJ/mol), which, by virtue of its relatively high value, excludes degradation mechanisms such as hydrogen embrittlement.

VI. DISCUSSION

A. K -Controlled Time-Dependent Crack Growth Models

Time-dependent crack growth is traditionally referred to as creep crack growth. It becomes apparent that TDCG in Ni-based superalloys can be the result of creep, oxidation, and stress corrosion. Quite a few models^[52,54,60–62] have been proposed for treating creep crack growth in Ni-based alloys. These creep crack growth models, which are summarized in several review

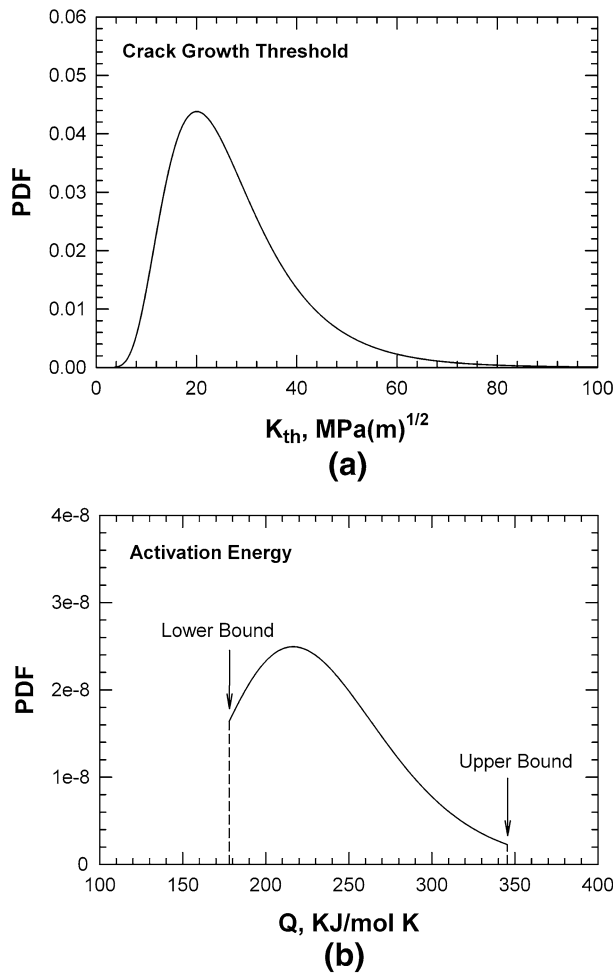


Fig. 16—Probability distribution functions used in the probabilistic crack growth analysis of cycle-dependent crack growth in an IN 718 disk with TDCG under diffusion-controlled conditions.

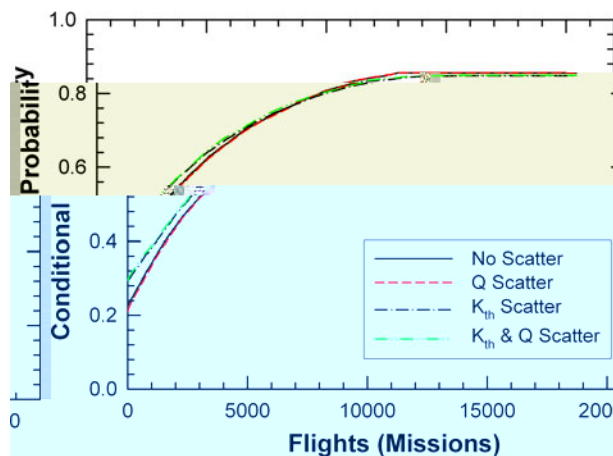


Fig. 17—Risk of disk fracture as a function of flight (mission) for cycle-dependent crack growth in an IN 718 disk with TDCG under diffusion-controlled conditions.

articles,^[52,60,62] consider creep crack growth to occur as the result of creep cavitation along grain boundaries ahead of a crack tip subjected to the near-tip stress field characterized by the K field or the time-dependent C_t

field. K -controlled creep crack growth is pertinent when the creep zone is small compared to other specimen dimensions. For some Ni-based alloys such as IN 718, TDCG is environmentally induced and the observed time-dependence effect is pronounced in air, but disappears in vacuum.^[59] Like small-scale creep, the TDCG is K -controlled and the crack growth kinetics can be correlated in terms of the K parameter when the size of the crack-tip oxidation zone is small and is entirely embedded within the K field. Under these circumstances, the time-dependent K -controlled crack growth model and the summation approach given by Eq. [20] is applicable. Contrarily, the time-dependent K -controlled model is not applicable when the creep or oxidation zone size is large. For Ni-based alloys such as IN 738 and IN 939 at 1123 K (850 °C),^[63] TDCG arises from both creep and oxidation at the crack tip. For this class of Ni-based alloys, the TDCG formulation requires two terms, one to represent damage due to plasticity (creep) and one to represent degradation due to oxidation, as in a recent model proposed by Ruiz-Sabariego and Pommier.^[64]

B. Microstructure-Based da/dt Model

In this study, a microstructure-based model has been developed for treating K -controlled crack growth in Ni-based alloys due to oxidation at high temperatures. The preliminary model predicts correctly the dependence of grain size on da/dt . The model also predicts decreases in the da/dt with increases in the yield strength and fracture strain ϵ_f . Since yield strength and fracture strain often obey an inverse relation, the exact dependence of da/dt on yield strength may be complicated and vary with individual alloys, depending on the effects of microstructure on yield strength and fracture strain. This aspect of the model has not been verified against experimental data and its validity requires further validation, but looks promising for incorporating the beneficial effects of decreasing da/dt by small γ' size commonly observed in Ni-based alloys^[59,65,66] and in the recently developed ALLVAC 718Plus alloy.^[67]

The K -controlled da/dt model, Eq. [4], is applicable to treating diffusion-controlled crack growth simply by setting $m = 0$ to arrive at the governing crack growth expression given by Eq. [6]. For diffusion-controlled crack growth, da/dt depends primarily on the activation energy, Q , and temperature. Experimental data for IN 718 indicates that the lower bound Q value corresponds to that for grain boundary diffusion, Q_{gb} . This lower bound is applicable for crack growth that accompanies the formation of non-protective oxides or creep cavities along the grain boundaries. Formation of protective oxides such as Cr_2O_3 and Al_2O_3 in the crack-tip process zone would increase the apparent Q value from $Q = Q_{gb}$ to $Q = 2Q_{gb}$, thereby reducing the crack growth rate. The analysis also indicates that caution must be exercised when the experimental Q values are fitted to a distribution function; in particular, a cutoff needs to be applied on the low-end side of the distribution in order to exclude extremely low activation energy values corresponding to degradation mechanisms

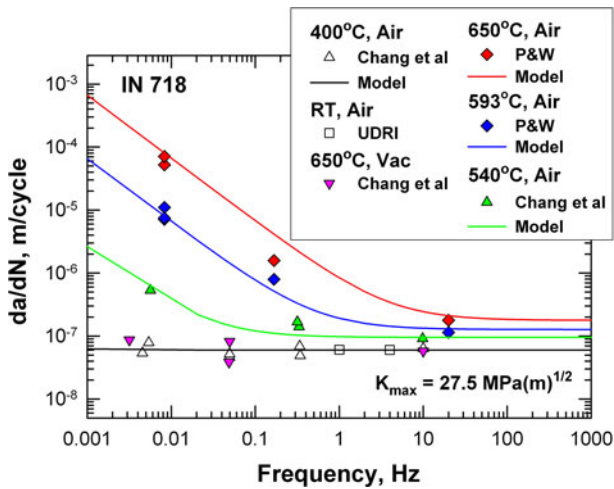


Fig. 18—Comparison of computed and measured da/dN as a function of frequency for various temperature and environments indicates TDCG is absent in vacuum at 923 K (650 °C). This finding indicates that TDCG in IN 718 in air is an environmentally induced phenomenon and that is not due to creep. The da/dt data are from References [5], [58], and [59]. From Chan *et al.*^[1]

such as hydrogen embrittlement that might not be present in service environments.

It is envisioned that Eq. [4] is also applicable for K-controlled creep crack growth in Ni-based alloys where degradation proceeds in the form of cavities formation at grain boundaries. Under this condition, the condition of $Q = Q_{gb}$ remains valid and da/dt is entirely determined by the pre-exponent term in Eq. [4]. In particular, the difference between creep crack growth and oxidation-induced crack growth lies in the critical strain term in Eq. [4]. The critical strain is expected to be larger for creep crack growth, but its value is reduced by the formation of brittle oxide particles within the crack-tip process zone. This rationale is supported by compilation of experimental data^[5,58,59] and model calculations, shown in Figure 18, which shows that TDCG occurs only in air at low frequency, but not in vacuum at 923 K (650 °C). The increase in da/dt at elevated temperatures and long time-durations can be interpreted as the result of decreases of the critical strain to fracture due to increased oxide formation in the crack-tip process over time.

The type of reactants and oxide products formed during the oxidation process appear to influence the critical strain to fracture and the threshold, K_{th} , for TDCG by virtue of the different magnitudes of the transformation stresses, as compressive transformation stresses are expected to delay, while tensile transformation stresses are expected to promote, oxide fracture. Results of this study have identified the sources of transformation stresses: (1) tensile transformation stresses originate from oxidation of grain boundary carbides (NbC, M_6C , and $M_{23}C_6$) and intermetallics (Ni_3Nb), and (2) compressive transformation stresses originate from oxidation of Ni solid-solution matrix and Ni_3Al . Based on the results on IN 718, it appears the oxidation of the Ni solid-solution phase and Ni_3Al dominates

since the observed K_{th} level is considerably higher than that based on the fracture toughness, K_{ox} , of the oxides. Although TDCG at elevated temperature has often been associated with creep, it has now become apparent that TDCG in Ni-based superalloys with grain boundary particles such as IN 718 is environmentally induced and mostly caused by grain-boundary oxidation since the enhanced TDCG occurs only in air, impure argon, or oxygen but disappears in vacuum, as shown in Figure 18. If the enhanced da/dt in Figure 18 was caused by crack-tip creep deformation, it would have occurred both in air and vacuum, not just in air alone.

C. DARWIN Life Assessments

In this investigation, life prediction and risk assessment have been made for a disk component subjected to a mission profile which contains long dwell durations at high service temperatures. The model constants were chosen to evaluate and to check the da/dt algorithm for diffusion-controlled crack growth with selected random variables. The important material variables for diffusion-controlled crack growth are the threshold, K_{th} , and the activation energy, Q . For both cases, the left tail of the distribution exerts a significant influence on the computed life and fracture risk. After investigating the potential origins of the low K_{th} , it was determined that the low end of the K_{th} distribution can physically arise from degradation mechanisms such as oxidation of grain boundary carbides (NbC, M_6C , and $M_{23}C_6$) or intermetallics (Ni_3Nb). Besides microstructural origins, the left tail of K_{th} can potentially depend on the load history used to determine the onset of TDCG. Unlike the cyclic crack growth threshold (ΔK_{th}), determination of K_{th} does not require unloading and its value is unaffected by the residual plastic strain in the crack wake. Instead, K_{th} is most likely dictated by oxide formation and fracture in the crack tip region and in the crack wake. Oxidation at the crack wake affects both the cycle threshold, (ΔK_{th}) and the static threshold (K_{th}). In this investigation, the effect of oxidation on the cyclic crack growth threshold, ΔK_{th} , was not considered. The TDCG rate, da/dt , is highly sensitive to the left tail of the Q distribution and the corresponding value for B_0 . Furthermore, the left tail of the Q distribution entails low Q values that are feasible only in the presence of degradation mechanism such as hydrogen embrittlement, which was considered unlikely for IN 718 because of the high K_{th} levels and the types of oxides formed. Thus, a cutoff was applied to limit the Q distribution to a lower bound of $Q = Q_{gb}$, which corresponds to the activation energy for grain boundary diffusion. Another material parameter that exhibits variability is the crack growth exponent m . For IN 718, m can range from 3 to nearly zero in the K-controlled crack growth regime when $K > K_{th}$. The effect of variability in m on the crack growth life, which can be important for K-controlled crack growth, will be evaluated in a future study. It was not evaluated in the current study because it would require substantial changes to the DARWIN code, which was beyond the scope of this investigation.

VII. CONCLUSIONS

The conclusions reached in this investigation are as follows:

1. A microstructure-based, TDCG model has been developed for treating oxidation corrosion, stress rupture, and creep crack growth. The microstructure-based model has the same form as the generic models for K-controlled and diffusion-controlled crack growth models.
2. Oxidation of the constituent phases in Ni-based alloys can lead to transformation stresses that exert compressive or tensile residual stresses in the crack-tip process zone, resulting in a wide range of K_{th} levels for the onset of TDCG.
3. Crack-tip oxidation of Ni solid-solution phase and Ni_3Al can lead to compressive transformation stresses, crack-tip shielding, and increases in the K_{th} level for TDCG.
4. Crack-tip oxidation of metal carbides and Ni_3Nb can lead to tensile transformation stresses, crack-tip anti-shielding, and decrease in the K_{th} level for TDCG.
5. A range of activation energy for TDCG can occur as the result of variations in the oxidation kinetics at the crack tip. The lower bound for the Q value for oxidation-induced crack growth is the activation energy for grain boundary diffusion, and its value is identical to that for creep crack growth.
6. A lower bound cutoff is required for the distribution of Q values in order to exclude Q values at the left tail of the distribution which corresponds to other degradation mechanisms not related to the crack-tip oxidation process.
7. DARWIN simulations indicate that diffusion-controlled TDCG can increase fracture risk in turbo-engine components under dwell fatigue conditions at high service temperatures.

ACKNOWLEDGEMENTS

This work was supported by NAVAIR under contract No. N68335-11-C-0171 and monitored by Mr. Raymond A. Pickering. The authors are thankful for the support of PW in providing the IN 718 data and the mission profile used in this study. The assistance by Ms. Lori Salas, SwRI, in the preparation of the manuscript is acknowledged.

APPENDIX

Oxidation at the crack tip is considered to occur within the damage zone, which is represented schemat-

ically by a crack-tip element of height d and width s in Figure 2. The plastic strain within the crack-tip element can be related to the crack-tip opening displacement, CTOD, and is approximated as^[68]

$$\varepsilon_{tip}^p \approx \frac{CTOD}{d} \quad \text{A1}$$

For small-scale yielding, CTOD is given by Reference 69

$$CTOD \approx \frac{K^2}{2\sigma_y E} \quad \text{A2}$$

which can be combined with Eq. [A1] to give

$$\varepsilon_{tip}^p \approx \frac{K^2}{2\sigma_y E d} \quad \text{A3}$$

Rearranging the terms in Eq. [2] leads one to

$$\frac{1}{t_f} \approx \frac{1}{t_o} \left(\frac{\varepsilon_p}{\varepsilon_f} \right)^{1/b} \quad \text{A4}$$

which is substituted into Eq. [1] to give

$$\frac{da}{dt} \approx \frac{s}{t_o} \left(\frac{\varepsilon_p}{\varepsilon_f} \right)^{1/b} \quad \text{A5}$$

which becomes

$$\frac{da}{dt} \approx \frac{s}{t_o} \left[\frac{1}{2\sigma_y E \varepsilon_f d} \right]^{\frac{m}{2}} K^m \quad \text{A6}$$

upon substituting Eqs. [A3] into [A5] and setting $m = 1/b$. The crack-tip element height d is assumed to be a function of the grain size, D , according to the expression given by Reference 70

$$d \approx d_o \left(\frac{D}{D_o} \right)^\gamma \quad \text{A7}$$

where D_o is a reference grain size, d_o is the crack-tip element height at the reference grain size D_o , and γ is an empirical constant. The crack-tip element width, s , is assumed to be related to the diffusive flow of oxygen atoms from the crack tip and is expressed as

$$s \approx s_o \exp \left(\frac{Q}{RT} \right) \quad \text{A8}$$

substituting Eqs. [A7] and [A8] into Eq. [4]. The proposed model, Eq. [4], is fairly complex and contains a large number of material constants including the yield stress (σ_y), critical fracture strain (ε_f), Young's modulus

Table AI. Model Constants for IN 718 at 923 K (650 °C) for Two Q Values

| E (GPa) | σ_y (MPa) | ε_f | d_o (nm) | D_o (μm) | D (μm) | s_o/t_o (mm/s) | m | γ | Theoretical B_o (mm/s{MPa(m) ^{1/2} } ^m) | Q (kJ/g mol) | Experimental B_o (mm/s{MPa(m) ^{1/2} } ^m) |
|--------------|---------------------|-----------------|---------------|----------------------------|--------------------------|---------------------|-------|----------|---|-------------------|--|
| 163.4 | 1000 | 0.22 | 2.6 | 1.0 | 30 | 2.75E+11 | 3.226 | 0.3100 | 7.49E+11 | 348.84 | 7.49E+11 |
| 163.4 | 1000 | 0.22 | 2.6 | 1.0 | 30 | 1.87E+05 | 3.226 | 0.3100 | 5.38E+05 | 241.3 | 5.11E+05 |

(E), grain size (D), and activation energy for grain-boundary diffusion (Q). There are also several empirical constants such as m , γ , s_o , t_o , and d_o . All of these parameters appear in the parameter B_o in Eqs. [6] and [7]. For evaluating material constants and applying the model, only the B_o parameter needs to be evaluated and individual contributors to B_o need not be evaluated if experimental data are not readily available. Table AI presents the model constants for IN 718 for various Q values. It is noted that the value for s_o/t_o was adjusted for a given Q value so that the computed B_o value matched the experimental B_o . The s_o/t_o value is correlated to the Q value and s_o/t_o cannot be predicted at this time.

REFERENCES

1. K.S. Chan, M.P. Enright, J.P. Moody, B. Hocking, and S.H.K. Fitch: *J. Eng. Gas Turbine Power*, 2012, vol. 134, p. 122501.
2. DARWIN[®] User's Guide. Southwest Research Institute, 2011, San Antonio, TX.
3. M. Prager and G. Sines: *ASME J. Basic Eng.*, 1971, vol. 225, pp. 225–30.
4. J.M. Larson and S. Floreen: *Metall. Trans. A*, 1977, vol. 8A, pp. 51–55.
5. Material data provided through direct telecommunications and in *Probabilistic Design for Rotor Integrity (PDRI) Interim Report 9*, Southwest Research Institute, March 4, 2010. The tests were performed by PW and funded under FAA Grant 05-G-005.
6. J.P. Pedron and A. Pineau: *Mater. Sci. Eng.*, 1982, vol. 56, pp. 143–56.
7. M. Gao, D.J. Dwyer, and R.P. Wei: *Superalloys 718, 625, 706 and Various Derivatives*, E.A. Loria, ed., TMS, Warrendale, PA, 1994, pp. 581–92.
8. R.P. Wei and Z. Huang: *Mater. Sci. Eng.*, 2002, vol. A336, pp. 209–214.
9. D.A. Woodford: *Energy Mater.*, 2006, vol. 1 (1), pp. 59–79.
10. S. Floreen and R. Raj: *Flow and Fracture at Elevated Temperatures*, ASM, Materials Park, 1983, pp. 383–404.
11. K. Sadananda and P. Shahinian: *Mater. Sci., Eng.*, 1980, vol. 43, pp. 159–68.
12. S. Floreen: *Metall. Trans. A*, 1975, vol. 17A, pp. 1741–49.
13. P.F. Browning: cited in Ref. [24] by D.A. Woodford: *Energy Mater.*, 2006, vol. 1 (1), pp. 59–79.
14. K. Sadananda and P. Shahinian: *Creep-Fatigue Environment Interactions*, R.M. Pelloux and N.S. Stoloff, eds., TMS-AIME, Warrendale, PA, 1979, pp. 86–111.
15. K. Sadananda and P. Shahinian: *J. Eng. Mater. Technol.*, 1978, vol. 100, pp. 381–87.
16. P. Valerio, M. Gao, and R.P. Wei: *Scripta Metall. Mater.*, 1994, vol. 30, pp. 1269–74.
17. X. Liu, B. Kang, W. Carpenter, and E. Barbero: *J. Mater. Sci.*, 2004, vol. 39, pp. 1967–73.
18. I. Gurrappa, S. Weinbruch, D. Naumenko, and W.J. Quadackers: *Mater. Corros.*, 2000, vol. 51, pp. 224–35.
19. R.M. McMeeking and A.G. Evans: *J. Am. Ceram. Soc.*, 1982, vol. 65, pp. 242–46.
20. H. Ghonem, T. Nicholas, and A. Pineau: *Fatigue Fract. Eng. Mater. Struct.*, 1993, vol. 16, pp. 577–90.
21. M. Olszta, D. Schreiber, L. Thomas, and S. Bruemmer: *Adv. Mater. Process.*, 2012, vol. 170 (4), pp. 17–21.
22. R. Cozar and A. Pineau: *Metall. Trans.*, 1973, vol. 4, pp. 47–59.
23. K. Kusabiraki, H. Komatsu, and S. Ikeuchi: *Metall. Mater. Trans. A*, 1998, vol. 29A, pp. 1169–74.
24. J.C. Zhao, V. Ravikumar, and A.M. Beltran: *Metall. Mater. Trans. A*, 2001, vol. 32A, pp. 1271–82.
25. T. Sourmail: *Mater. Sci. Technol.*, 2001, vol. 17, pp. 1–14.
26. T.M. Pollock and S. Tin: *J. Propuls. Power*, 2006, vol. 22, pp. 361–74.
27. J. Laigo, F. Tancret, R. Le Gall, and J. Furtado: *Adv. Mater. Res.*, 2007, vols. 15–17, pp. 702–07.
28. W. Acchar and C.A. Cairo: *Mater. Res.*, 2006, vol. 9, pp. 171–74.
29. K. Koji, N. Yokotani, and Y. Umakoshi: *Mater. Sci. Forum*, 2006, vol. 512, pp. 67–72.
30. K. Hirota, K. Mitani, M. Yoshinak, and O. Yamaguchi: *Mater. Sci. Eng. A*, 2005, vol. 399, pp. 154–60.
31. G.A. Young, T.E. Capobianco, M.A. Penik, B.W. Morris, and J.J. McGee: *Weld. J.*, 2008, vol. 87, pp. 31s–43s.
32. J.D. Rigney and J.J. Lewandowski: *Mater. Sci. Eng. A*, 1992, vol. 149, pp. 143–51.
33. S. Musikant: *What Every Engineer Should Know About Ceramics*, chap. 6, Marcel-Dekker, New York, NY, 1991, pp. 99–122.
34. T. Chudoba, N. Schwarzer, and F. Richter: *Surf. Coat. Technol.*, 2000, vol. 127, pp. 9–17.
35. D. Tromans and J.A. Meech: *Miner. Eng.*, 2002, vol. 15, pp. 1027–41.
36. J.A. Crawford: *J. Appl. Phys.*, 1964, vol. 35, pp. 2413–18.
37. P. Thompson, D.E. Cox, and J.B. Hastings: *J. Appl. Crystallogr.*, 1987, vol. 20, pp. 79–83.
38. H. Berger, H. Tang, and F. Levy: *J. Cryst. Growth*, 1993, vol. 130, pp. 108–12.
39. C. Yan and D. Yue: *Adv. Mater.*, 2008, vol. 20, pp. 1055–58.
40. D.R. Lide: *CRC Handbook of Chemistry and Physics*, 79th ed., CRC, Boca Raton, FL, 1998/1999.
41. T. Bredow and A.R. Gerson: *Phys. Rev. B*, 2000, vol. 61, pp. 5194–201.
42. X.S. Du, S. Hak, T. Hibma, O.C. Rogojanu, and B. Struth: *J. Cryst. Growth*, 2006, vol. 293, pp. 228–32.
43. R. Guillaumont, J. Lopitiaux, B. Hannoyer, and M. Lenglet: *J. Phys. IV*, 1993, vol. 3, pp. 349–56.
44. R.W. Hertzberg: *Deformation and Fracture Mechanics of Engineering Materials*, Wiley, New York, 1976, p. 8.
45. W.J. Mills and L.D. Blackburn: *J. Eng. Mater. Technol.*, 1988, vol. 110, pp. 286–97.
46. Y.H. Qi, P. Bruckel, and P. Lours: *J. Mater. Sci.*, 2003, vol. 22, pp. 371–74.
47. L.A. James and W.J. Mills: *Eng. Fract. Mech.*, 1985, vol. 22, pp. 797–817.
48. J.L. Yuen, C.G. Schmidt, and P. Roy: *Fatigue Fract. Eng. Mater. Struct.*, 1985, vol. 8, pp. 65–76.
49. S. Suresh and R.O. Ritchie: *Scripta Metall.*, 1983, vol. 17, pp. 575–80.
50. S.J. Hudak, Jr. and R.A. Page: *Corrosion*, 1983, vol. 39, pp. 285–90.
51. J.L. Yuen, P. Roy, and W.D. Nix: *Metall. Trans. A*, 1984, vol. 15A, pp. 1769–75.
52. S.S. Kim, S.J. Choe, and K.S. Shin: *Met. Mater.*, 1998, vol. 4 (1), pp. 15–23.
53. R.P. Wei and J.D. Landes: *Mater. Res. Stand.*, 1969, vol. 44 (46), pp. 25–27.
54. R.H. Van Stone and D.C. Slavik: *Fatigue and Fracture Mechanics: 31st Volume, ASTM STP 1389*, G.R. Halford and J.P. Gallagher, eds., ASTM, West Conshohocken, PA, 2000, pp. 405–26.
55. P.C. Paris and F. Erdogan: *Trans. ASME J. Basic Eng. Ser. D*, 1963, vol. 85 (3), pp. 528–533.
56. R.W. Hayes: *Metall. Mater. Trans. A*, 2008, vol. 39A, pp. 2596–606.
57. M.J. Starink and P.A.S. Reed: *Mater. Sci. Eng. A*, 2008, vol. 491, pp. 279–89.
58. T. Weerasooriya: *AFWAL-TR-4038*, University of Dayton, Dayton, OH, June 1987.
59. K.-M. Chang, M.F. Henry, and M.G. Benz: *JOM*, 1990, vol. 42 (12), pp. 29–35.
60. S.S. Kim, S.J. Choe, and K.S. Shin: *Met. Mater.*, 1998, vol. 4, pp. 1–13.
61. K.O. Findley, J.L. Evans, and A. Saxena: *Int. Mater. Rev.*, 2011, vol. 56, pp. 49–71.
62. C.M. Branco, A.S. Brito, and J. Byrne: *Proceedings of TRO AVT Workshop on "Qualification of Life Extension Schemes for Engine Components"*, Corfu, Greece, October 1998.
63. W. Hoffelner: *Mater. Sci. Technol.*, 1987, vol. 3, pp. 765–70.
64. J.A. Ruiz-Sabariago and S. Pommier: *Int. J. Fatigue*, 2009, vol. 31, pp. 1724–32.
65. J. Telesman, P. Kantzos, J. Gayda, P.J. Bonacuse, and A. Prescenzi: *Superalloys 2004*, K.A. Green, T.M. Pollock, H. Harada, T.E. Howson, R.C. Reed, J.J. Schirra, and S. Walston, eds., TMS, Warrendale, PA, 2004, pp. 215–24.

66. D. Rice, P. Kantzos, B. Hann, J. Neumann, and R. Helmink: *Superalloys 2008*, R.C. Reed, K.A. Green, P. Caron T.P. Gabb, M.G. Fahrman, E.S. Huron, and S.A. Woodard, eds., TMS, Warrendale, PA, 2008, pp. 139–47.
67. J. Tsang, R.M. Kearsey, P. Au, S. Oppenheimer, and E. McDevitt: *Can. Metall. Q.*, 2011, vol. 50 (3), pp. 222–31.
68. J.R. Rice: *J. Appl. Mech.*, 1968, vol. 35, pp. 379–86.
69. D. Broek: *Elementary Engineering Fracture Mechanics*, Sijthoff & Noordhoff, Alphen aan den Rijn, the Netherlands, 1978, pp. 218–19.
70. M.P. Enright and K.S. Chan: *J. ASTM Int.*, 2004, vol. 1 (8), pp. 87–103.